

Electronic Supporting Information

Synthesis and Testing Methodologies:

NbOPO₄ used in this work was prepared according to the literature.^[1] In a typical synthesis of NbOPO₄, 1.32 g (0.01 mol) of diammonium hydrogen phosphate was dissolved in 20 ml water and then adjusted pH to 2 using phosphoric acid. With vigorous stirring, 20 ml of 0.5 M niobium oxalate (pH=2) was added to the above solution. Then the mixed solution was dropped into the aqueous solution of cetyltrimethyl ammonium bromide (CTAB) which was previously prepared by dissolving 1.0 g of CTAB in 15 mL of distilled water. The pH value of the final solution was about 2. Afterwards, this mixture was stirred for additional 60 min at 35 °C, and then the solution was aged in a Teflon-lined autoclave for 24 h at 160 °C. After cooled down, the solid was filtered, washed with distilled water and then dried at 50 °C overnight. Finally, NbOPO₄ sample was obtained by calcination at 500 °C for 5 h in air with a linear heating ramp of 1 °C·min⁻¹ to remove organic species.

Bifunctional catalysts (Pt/NbOPO₄, Pd/NbOPO₄, Pd/H-Beta) were prepared by incipient wetness impregnation of the supports with the aqueous solution of Pt(NO₃)₂·xH₂O, Pd(NO₃)₂·xH₂O respectively. After impregnation, the catalysts were dried at 100 °C for 12 h, followed by calcination in air at 500 °C for 3 h with a linear heating ramp of 1 °C·min⁻¹.

The hydrodeoxygenation reactions were all conducted in a 300 mL Teflon-lined Parr reactor. In a typical run, feedstock (0.60 g), catalyst (0.20 g), and cyclohexane (30 mL) were put into the reactor, which was then sealed, purged three times with H₂ and charged to an initial pressure (30 bar). The reactor was then slowly heated to the reaction temperature (180 °C) under vigorous stirring and held for 24 h. After the reaction finished, the reactor was quenched in an ice/water bath. The gas phase was carefully collected in a gas bag and analysed by GC equipped with a packed column, a methaniser (for CO₂ detection) and a flame ionisation detector (FID). The products in the liquid phase were qualitatively analysed by GC-MS and quantitatively analysed by GC-FID equipped with a SCG-1 column. The yields of liquid alkanes were determined by adding dodecane as an internal standard after reaction. Mass yields were calculated by the equation: mass yield of alkanes = (mass of alkanes)/(mass of feedstock input). Carbon yields of liquid alkanes were calculated by the equation: carbon yield of alkanes = (mass of carbon in alkanes)/(mass of carbon in fatty acid). Carbon yield of propane was calculated by the equation: carbon yield of propane = (mass of carbon in propane) / (mass of carbon in glycerol part).

It is noted that the biodiesel has a reduced viscosity in comparison to vegetable oil. However, in comparison to the conventional petroleum diesel, FAME still has a relatively higher viscosity and poorer flow quality at low temperature, which limits its direct application as a high grade fuel.

(Fuel, 2008, 87, 2069–2075; Green Chem., 2013, 15, 1720–1739). Thus, the approach of producing alkanes from hydrogenolysis of vegetable oil is more advantageous than that of conventional biodiesel in terms of physical properties.

EXAFS experiment:

Local structures surrounding Nb atoms were probed by using extended x-ray absorption fine structure (EXAFS) technique at beamline BL07A of Taiwan Light Source at National Synchrotron Radiation Research Center (NSRRC) in Taiwan. A Si(111) Double Crystal Monochromator (DCM) was used to scan the photon energy. The energy resolution ($\Delta E/E$) for the incident X-ray photons was estimated to be 2×10^{-4} . Conventional transmission mode was adopted for Nb K-edge EXAFS measurements. To ascertain the reproducibility of the experimental data, at least two scan sets were collected and compared for each sample. The EXAFS data analysis was performed using IFEFFIT 1 with Horae packages 2 (Athena and Artemes). The spectra were calibrated with foils as a reference to avoid energy shifts of the samples. And the amplitude parameter was obtained from EXAFS data analysis of the foil, which was used as a fixed input parameter in the data fitting to allow the refinement in the coordination number of the absorption element. In this work, the first shell data analyses under the assumption of single scattering were performed with the errors estimated by R-factor.

TMP-adsorbed sample preparation and ^{31}P MAS NMR experiments:

150 mg of reduced Pd/NbOPO₄ sample was placed in a home-made glass tube and activated at 573 K for 2 h under vacuum (10^{-1} Pa). After cooling down to room temperature, a certain amount of TMP was introduced into this system and the glass tube was immersed in liquid nitrogen for promoting the adsorption of TMP. Prior to Nuclear Magnetic Resonance (NMR) experiment, the sample was transferred into a Bruker 4 mm ZrO₂ rotor with a Kel-F endcap in a glove box under dry nitrogen atmosphere. Solid state magic angle spinning (MAS) NMR experiments were carried out on a Bruker Avance III 400WB spectrometer at room temperature. The Larmor frequency is 162.1 MHz for ^{31}P . ^{31}P MAS NMR spectra were recorded with a 30° pulses, a recycle delay of 15 s and a MAS speed of 12 kHz. The ^{31}P chemical shifts were reported relative to 85% aqueous solution of H₃PO₄, with NH₄H₂PO₄ as a secondary standard (0.81 ppm).

Computational details:

All the calculation were carried out using the Vienna ab initio simulation package (VASP), and the exchange-correlation term was described by the Perdew, Burke, and Ernzerhof version within the generalized gradient approximation (PBE-GGA). The project-augmented wave (PAW) method was used to represent the core-valence electron interaction. The calculations were also conducted

involving Van De Waals force corrections. The Nb 4s, 4p, 4d, 5s, O 2s, 2p, C 2s, 2p and H 1s electrons were treated as valence electrons, and an energy cutoff of 400 eV for the basis-set expansion was used. The Nb₂O₅(001) surfaces was modeled as a periodic slab with six layers (about 17 Å thick). A p(3×3) super cell (surface area of 11.95 × 11.48 Å²) and a ~15 Å vacuum gap perpendicular to the surface was employed in the calculations, with a corresponding 1×1×1 k-point mesh. All the atoms were allowed to relax except those at the bottom layer until atomic forces reached below 0.05 eV/Å.

Calculation of the theoretical maximum mass yield of diesel-range alkanes from vegetable oils

Table S1 The detailed composition (fatty acids) of palm oil and soybean oil.

Feedstock	Fatty acids (wt %)					
	Myristic acid C14:0	Palmitic acid C16:0	Linolenic acid C18:3	Linoleic acid C18:2	Oleic acid C18:1	Stearic acid C18:0
Palm oil	0.5-6	35-48	0	6-13	35-50	3-7
Soybean oil	0	11.19	8.84	58.16	18.24	3.58

For the theoretical maximum mass yield of vegetable oils, we first assume that all of the fatty acids are from triglycerides, because in this case the glycerol part account for the minimum mass percentage.

Therefore, the theoretical mass yield from myristic acid triglycerides is: $198.4 \times 3 / 723.4 = 82.3\%$

from Palmitic acid triglycerides is: $226.4 \times 3 / 807.5 = 84.1\%$

from Linolenic acid triglycerides is: $254.5 \times 3 / 873.5 = 87.4\%$

from Linoleic acid triglycerides is: $254.5 \times 3 / 879.5 = 86.8\%$

from Oleic acid triglycerides is: $254.5 \times 3 / 885.5 = 86.2\%$

from Stearic acid triglycerides is: $254.5 \times 3 / 891.5 = 85.6\%$

As for palm oil: according to average value in Table S1, the palm oil contains 3, 41, 0, 8.5, 42.5, 5 wt% (total 100 wt%) of myristic acid, palmitic acid, linolenic acid, linoleic acid, oleic acid and stearic acid, respectively. therefore, the theoretical mass yield from **palm oil** is:

$$82.3\% \times 3\% + 84.1\% \times 41\% + 86.8\% \times 8.5\% + 86.2\% \times 42.5\% + 85.6\% \times 5\% = \mathbf{85.2\%}$$

For soybean oil, according to Table S1, the theoretical mass yield from **soybean oil** is: $84.1\% \times 11.19\% + 87.4\% \times 8.84\% + 86.8\% \times 58.16\% + 86.2\% \times 18.24\% + 85.6\% \times 3.58\% = \mathbf{86.4\%}$

The mass or carbon yield is commonly used in literature due to the fact that such value is industrially more relevant. For example, the carbon yield of alkanes formed from soybean oil is defined as carbon content in alkanes/carbon content in the three fatty acid parts of the soybean oil; the carbon yield of propane formed is defined as carbon content in propane/carbon content in glycerol of the triglyceride. 86.4% carbon yield towards alkanes and 80% carbon yield of glycerol towards propane. Thus, the near stoichiometry of 3: 1 can be worked out.

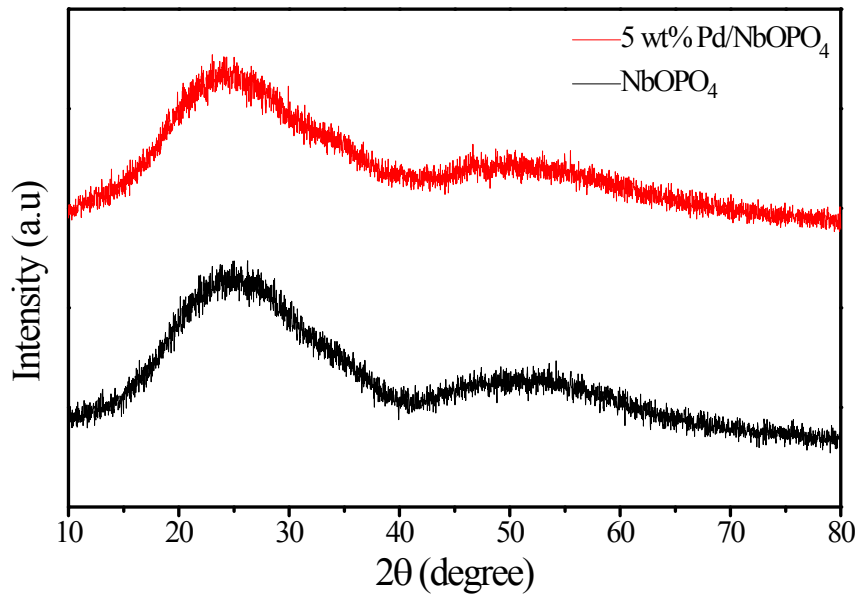


Figure S1 X-ray diffraction (XRD) patterns of NbOPO₄ and reduced 5 wt% Pd/NbOPO₄.

The XRD pattern of reduced 5 wt% Pd/NbOPO₄ shows glassy nature and almost the same with the support NbOPO₄, with no obvious characteristic peaks of Pd, indicating the well-dispersion of Pd particle.

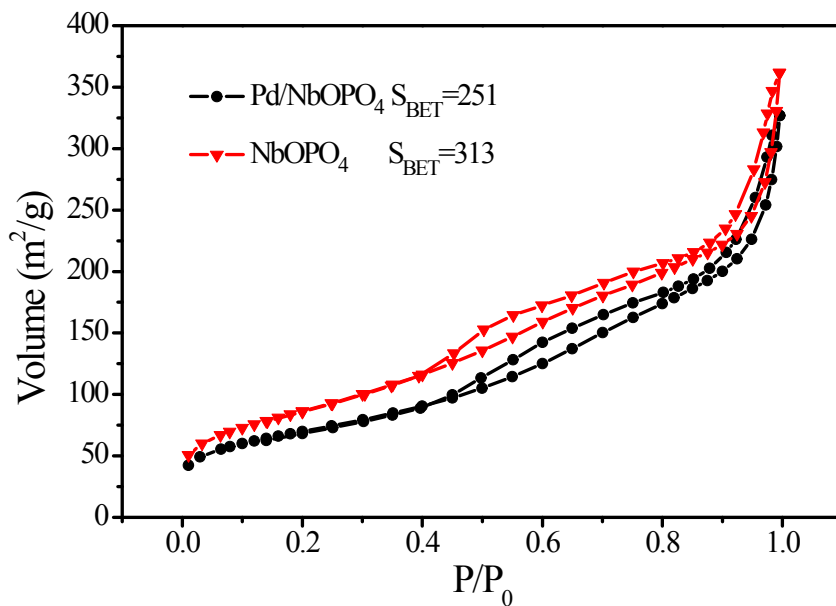


Figure S2 N₂ adsorption/desorption isotherm of NbOPO₄ and 5 wt% Pd/NbOPO₄. The N₂ adsorption-desorption isotherms of NbOPO₄ materials exhibit a typical type IV isotherm, which is a characteristic of mesoporous materials. The appearance of H2-type hysteresis loops at relative pressure 0.4-0.8 indicates the presence of “ink bottle”-type pores in these materials.

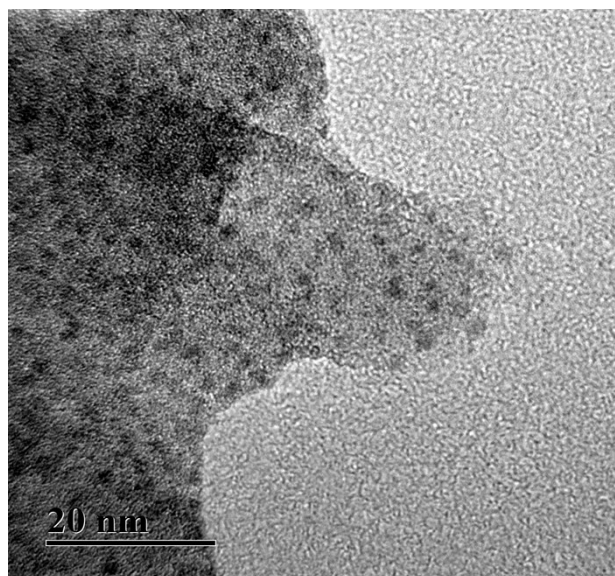


Figure S3 TEM image of 5 wt% Pd/NbOPO₄. TEM image of reduced 5 wt% Pd/NbOPO₄ catalyst shows that the Pd is well-dispersed on the NbOPO₄ support. The average size of Pd particle is about 3-4 nm.

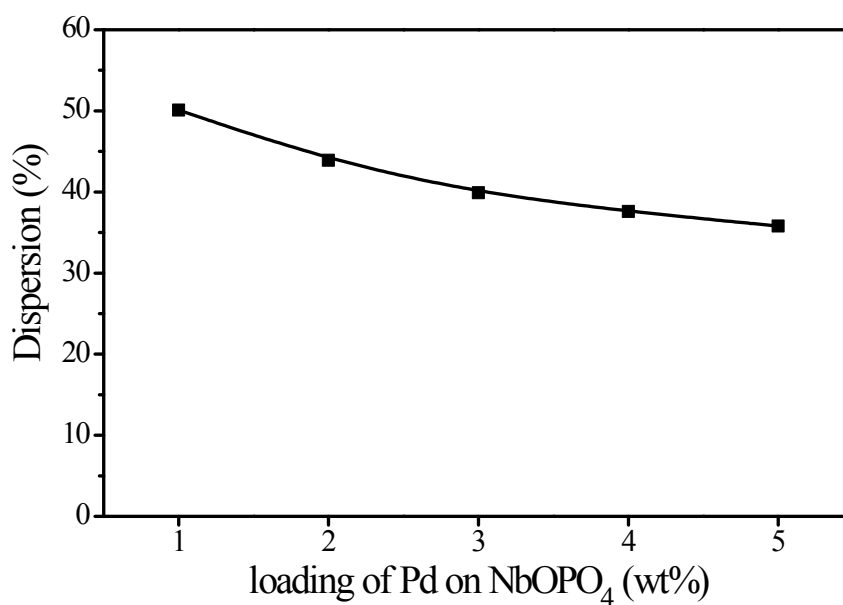


Figure S4 Pd dispersion of Pd/NbOPO₄ catalysts with different Pd loading

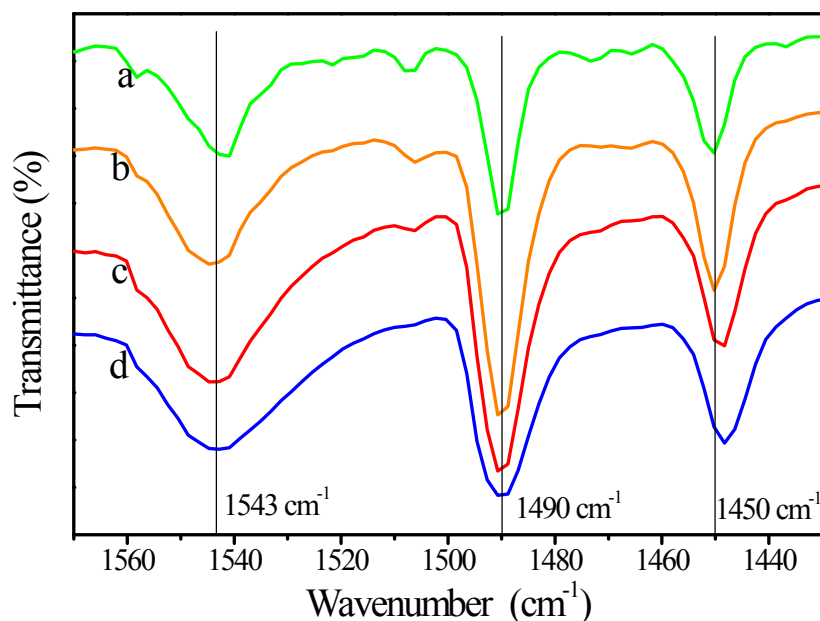
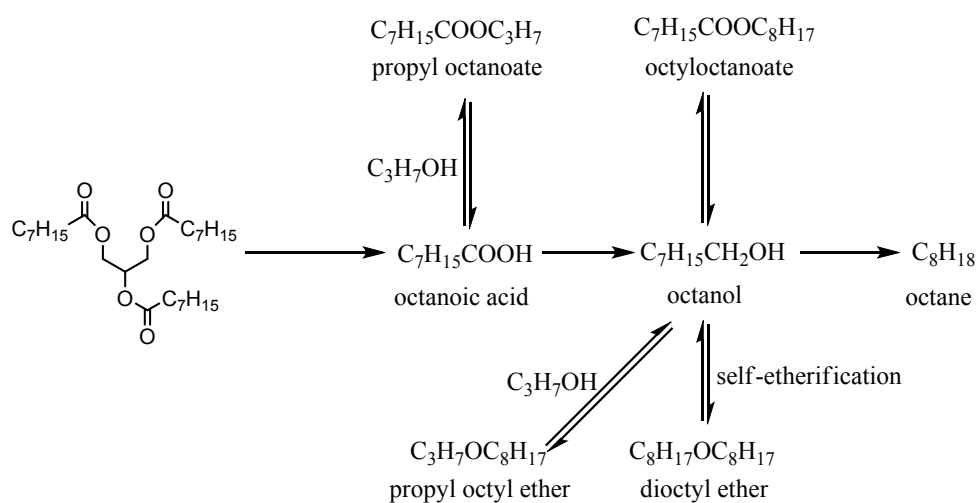


Figure S5 Pyridine-FTIR spectra of NbOPO₄ obtained after desorption at (a) 400 °C (b) 300 °C (c) 200 °C and (d) 100 °C. The band at 1450 cm⁻¹ can be attributed to the adsorption of pyridine on Lewis acid sites, the band at 1490 cm⁻¹ can be assigned to the adsorption of pyridine at both Brönsted and Lewis acid sites, and the band at 1543 cm⁻¹ (slightly shift to high wavenumber) corresponds to the adsorption of pyridine at Brönsted acid sites. These results indicate that NbOPO₄ possesses both Brönsted and Lewis acid sites.



Scheme 1. The proposed reaction pathways of glyceryl trioctanoate conversion.

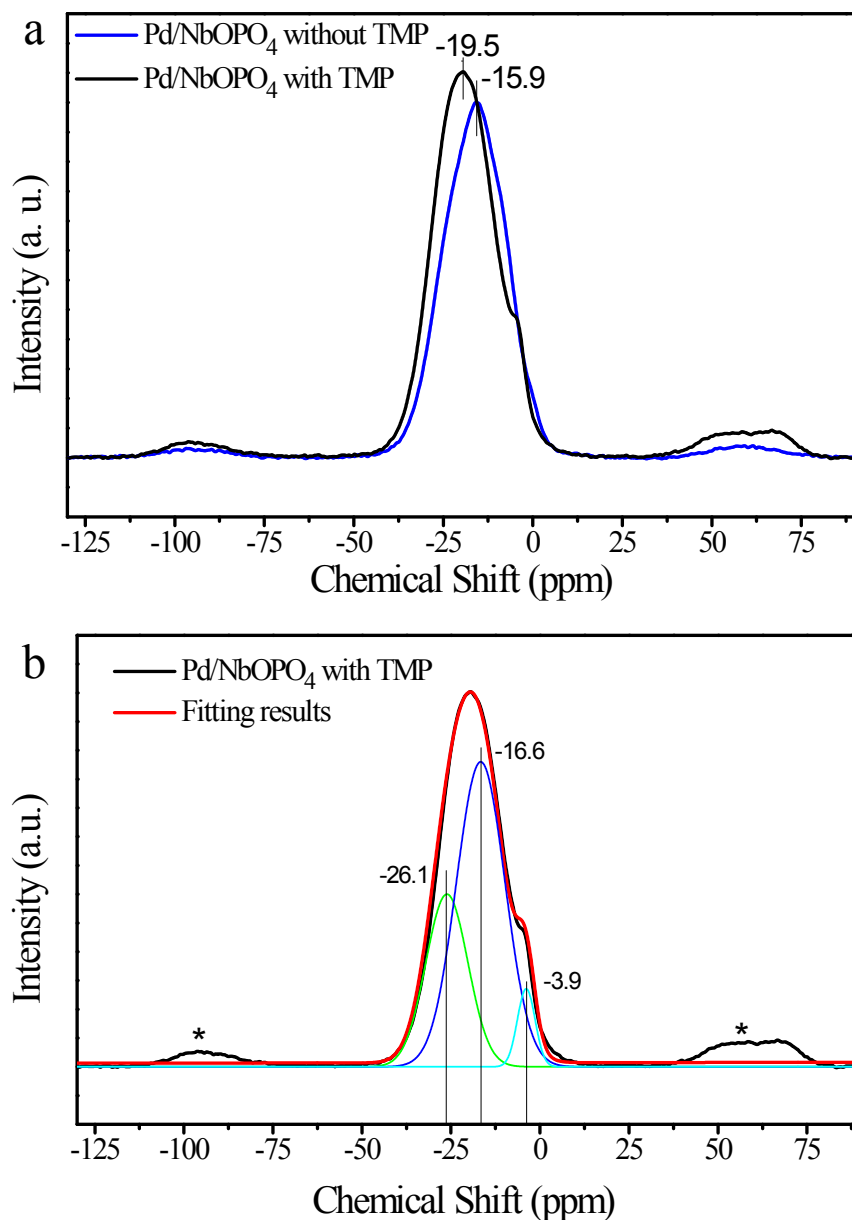


Figure S6a: ^{31}P MAS NMR spectra of reduced Pd/NbOPO₄ with/without (CH₃)₃P (TMP) adsorption. **S6b:** the spectrum deconvolution of TMP-adsorbed reduced Pd/NbOPO₄.

Generally, adsorbed TMP molecules react with BA sites to form TMPH⁺ giving rise to a ^{31}P chemical shift ($\delta^{31}\text{P}$) from -2 to -5 ppm, while TMP molecules bind to LA sites result in the range from ca. -20 to -60 ppm. As TMP, an electron donor molecule (Lewis base, LB), is expected to form adduct bond with exposed cation (Lewis acid, LA), the formation of TMP-LA complex may be realized by the coordination of the P atom at a LA center. The existence of LA site on reduced Pd/NbOPO₄ was therefore confirmed by evaluating its interaction with TMP. As shown in Figure S6a, the upfield 3 ppm shift of the reduced Pd/NbOPO₄ while introducing TMP (from -15.9 to

-19.5) clearly indicates the existence of coordinated unsaturated Nb (Lewis acid site). Further spectrum deconvolution of TMP-adsorbed reduced Pd/NbOPO₄ (Figure S6b) gives three peaks at -26.1, -16.6 and -3.9 ppm. As the peak at -3.9 ppm is assigned to surface BA site and the phosphor of NbOPO₄ gives a signal at around 16 ppm, the peak appeared at upfield (-26.1 ppm) is, therefore, ascribed to TMP coordinated with LA. It is surprising that the strength of this LA site is comparable to well-known super solid acid catalysts such as SO₄²⁻/ZrO₂,^[2] SO₄²⁻/TiO₂,^[3] BF₃/Al₂O₃.^[4]

Catalyst	$\delta^{31}\text{P}$ of Bronsted site	$\delta^{31}\text{P}$ of Lewis site	Reference
SO ₄ ²⁻ /ZrO ₂	-3.8 ppm	-33.7; -39.7; -44.4 ppm	2
SO ₄ ²⁻ /TiO ₂	-4 ppm	-24 ppm	3
BF ₃ /Al ₂ O ₃	-3.4 ppm	-41; -53 ppm	4

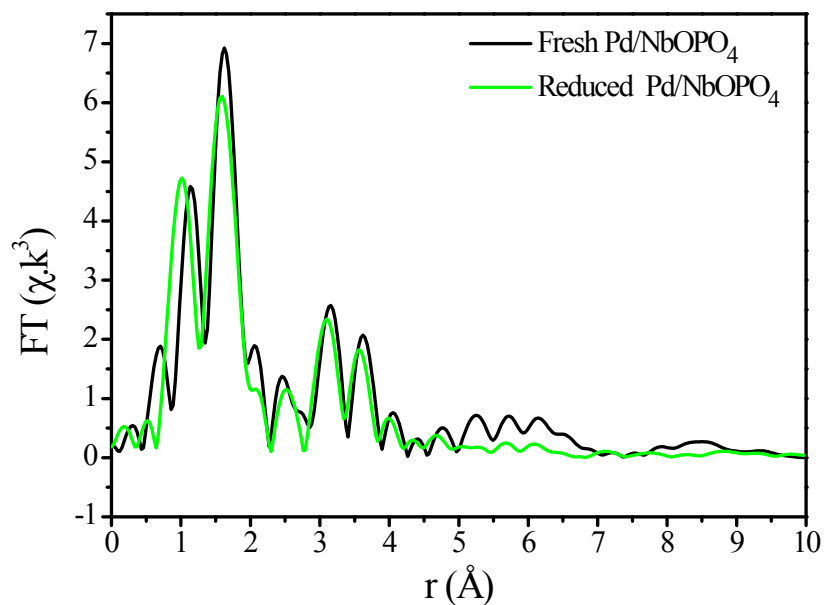


Figure S7 k^3 -EXAFS curves versus radial distance of Pd/NbOPO₄ before (black) and after (green) reduction: a substantial peak shift to shorter distance at 1.5 Å is noted.

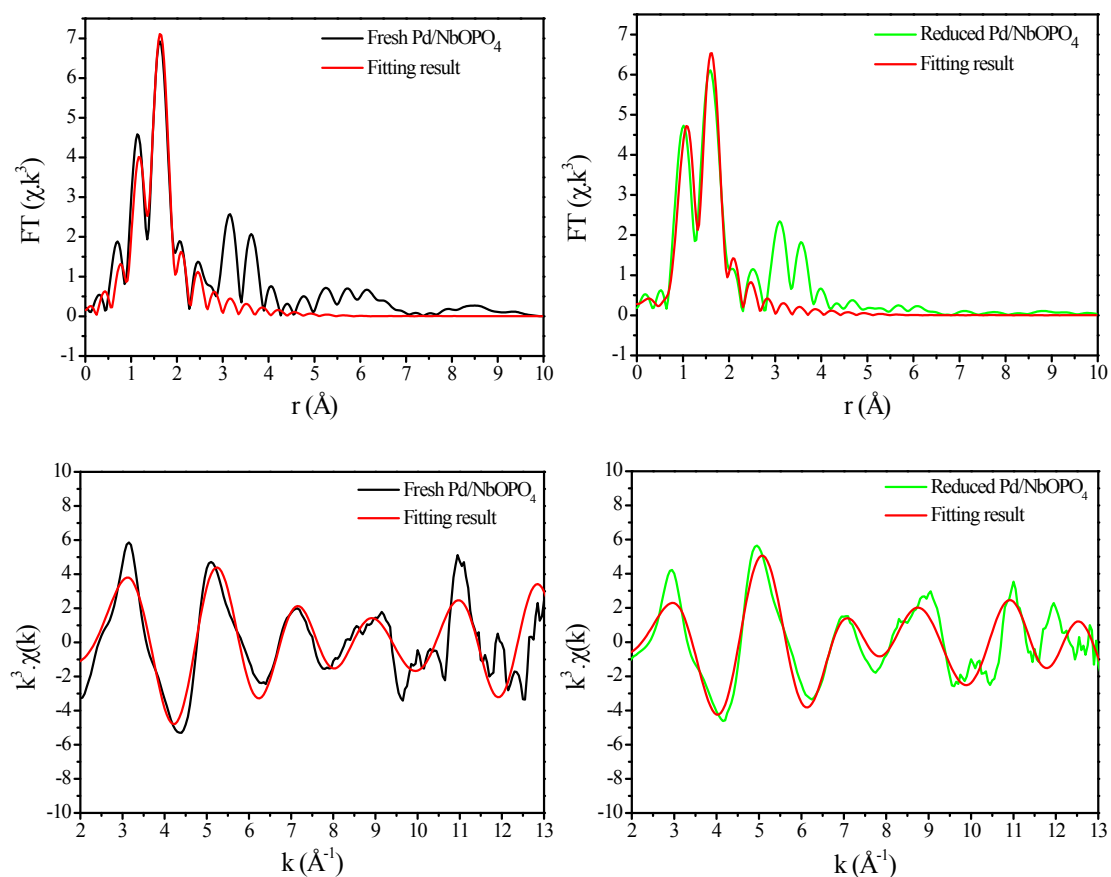


Figure S8 EXAFS plot of : $k^3 \cdot \chi$ phase corrected Fourier transform of experimental and fitting result for (a) fresh and (b) reduced Pd/NbOPO₄; $k^3 \cdot \chi$ experimental and fitting result for (c) fresh and (d) reduced Pd/NbOPO₄.

Table S2 EXAFS fitting parameters of fresh and reduced Pd/NbOPO₄

Sample	Shell	Bond length (Å)	Coordination number	σ^2 (Å ²)	ΔE (eV)	R factor (%)
Fresh Pd/NbOPO ₄	Nb-O1	1.80 (1)	1.1 (2)	0.002 (1)	8	2.6
	Nb-O2	1.98 (1)	4.0 (2)	0.004 (1)		
	Nb-O3	2.52 (3)	1.0 (3)	0.002 (1)		
Reduced Pd/NbOPO ₄	Nb-O1	1.82 (1)	1.0 (1)	0.002 (1)	8	3.0
	Nb-O2	2.00 (1)	3.4 (1)	0.003 (1)		
	Nb-O3	2.52 (1)	0.8 (1)	0.002 (1)		
	Nb-O4	1.41 (2)	0.4 (1)	0.002 (1)		

From the best fit data the reduced sample gives characteristic shorter bond of 1.41 Å with CN of 0.4. This peak distance as compared to typical Nb=O of 1.6 Å may have been underestimated due to larger fitting errors in this region owing to backscattering by the nearest oxygen atoms.^[14] Nevertheless, the formation of this shorter bond is clearly at the expense of longer bonds of Nb-O3 (CN decrease from 4 to 3.4) and Nb-O4 (CN decrease from 1 to 0.8) with total decrease of average CN from 6.1 to 5.6, indicative of reduction of [O] from the structure within experimental errors.

The XPS results of fresh and used catalysts

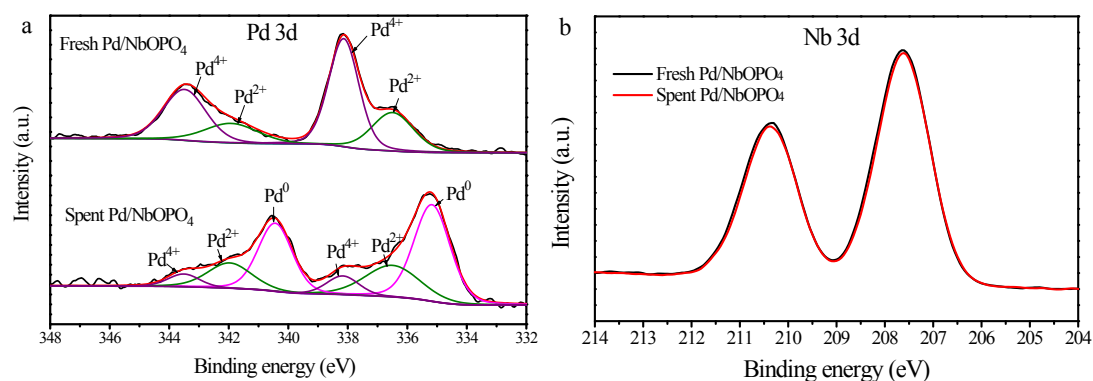


Figure S9 the XPS spectra of fresh and used catalysts. a) Pd 3d scan, b) Nb 3d scan. X-ray photoelectron spectroscopy (XPS) results of the fresh and spent sample were recorded on Thermo Escalab 250 spectroscopy with a monochromatic Al K α X-ray source. All binding energies were referenced to the C 1s peak (284.8 eV) arising from the adventitious carbon.

As seen from the above figure, the XPS spectra of Pd 3d before and after reaction show that Pd was clearly reduced after reaction, but a small amount of Pd²⁺ and Pd⁴⁺ existed presumably due to air re-oxidation of the sample during the transfer for the measurement. The XPS spectra of Nb 3d show almost the same positions before and after reaction. This could be due to two reasons: 1) the used catalyst was rapidly re-oxidized in air during the transfer of the sample as the reversed phenomenon was observed in the TPR experiment since replenishment and formation of surface oxygen vacancies of this material are readily taken place at room temperature. 2) the amount of surface oxygen vacancies was too small to visualize the shift of Nb 3d peaks. Further effort would be required in using in-situ XPS to address the fast redox properties of the Pd/NbOPO₄ phase.

Theoretical Calculations:

For surface reactions, first, we consider two adsorption forms (Figure S11): carbonyl oxygen adsorption (O_a adsorption, IS1) and ether oxygen adsorption (O_b adsorption, IS2). In the calculated structure (IS1), O_a bond to Nb atom with an adsorption energy of 1.12 eV, the C_1-O_b bond is activated and increased by 0.014 Å (from 1.458 Å to 1.472 Å) while the C_2-O_b bond is shorted by 0.032 Å (from 1.364 Å to 1.332 Å), indicating that C_2-O_b bond is not likely to break. Considering the C_1-O_b bond break with a high energy barrier of 1.96 eV, we believe O_a adsorption is disadvantage to the following bond breaking process. For O_b adsorption structure (IS2), O_b interacts with surface niobium atom with adsorption energy of 1.16 eV. At the same time, C_1-O_b bond is increased by 0.022 Å (from 1.458 Å to 1.480 Å) and C_2-O_b bond is increased by 0.036 Å (from 1.364 Å to 1.400 Å), both are thus activated. For the two intermediate structure formed by breaking the above two bonds, the calculated activation energy of TS2 (break C_1-O_b) is 2.34 eV, while an extremely low energy of 0.84 eV for TS3 (break C_2-O_b). Even though intermediate structure IM1 is 0.2 eV more stable than IM2, the reaction could still occurs much easier by break C_2-O_b bond. In particular, the synergism of the Lewis acid property of surface Nb cation and the strong inherent stress release trend of Nb-O-Nb chain makes it readily for the C-O bond activation and breakage of adsorbed ethyl butyrate molecule. The interesting thing is that the adsorb species of two intermediate structures are exactly similar: both were adsorbed butyrate specie and adsorbed ethoxy specie. In structure IM2, the butyrate specie adsorb on a niobium atom, the ethoxy specie adsorb on oxygen vacancy with its oxygen atom bond to another niobium atom next to the butyrate adsorbed one. Whereas for IM3, the adsorption sites of the two adsorbed species are contrary to that of IM2. It is worth noting that the energy difference between the two intermediate structures is only 0.2 eV, thus we believe that the two structures can transform to each other.

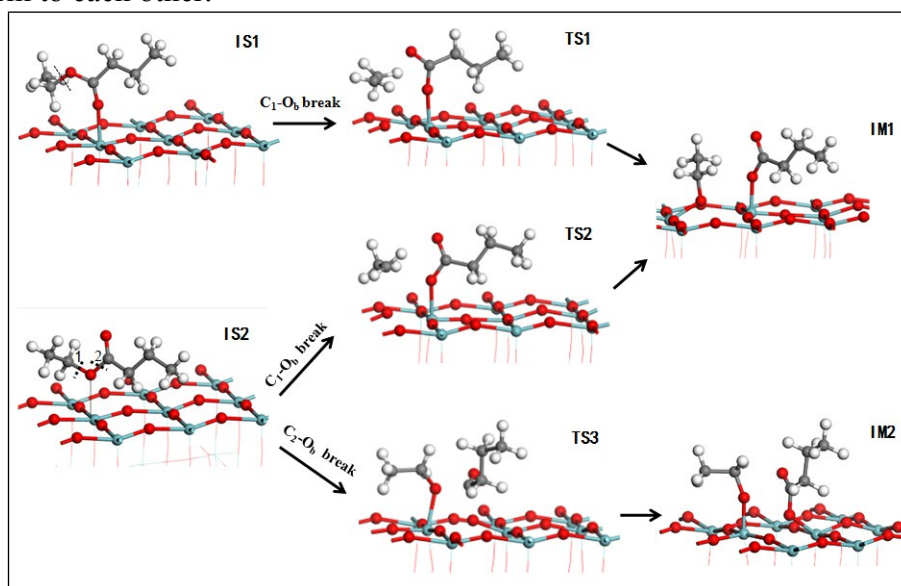
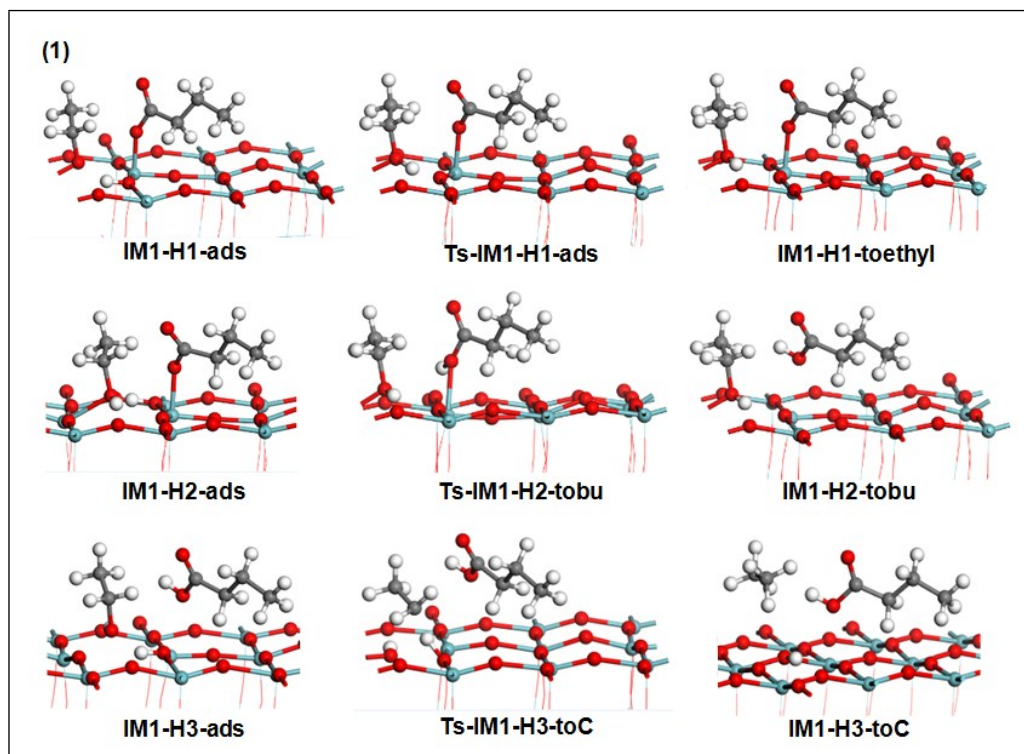


Figure S11. Calculated structures of model molecule adsorption and C-O bond break process. The Nb atoms are shown in light blue, O in red, C in black, and H in white.

We then calculated the subsequent hydrogenation processes of adsorbed ethoxy specie and butyrate specie of the two intermediate structures. It is well known that Pd has a good ability of dissociating H_2 , the dissociated hydrogen atoms can spillover to support surface. Herein we assumed that H_2 can readily dissociate at Pd and then transfer to the Nb_2O_5 support surface. For the more stable intermediate structure IM1, as we can see, the first hydrogen atom favors bonding to O_{2C} beside the Nb-O bond of adsorbed butyrate with a negative adsorption energy of -0.26 eV, which indicate that the hydrogen atom is unstable. By performing climbing image nudged elastic band (CI-NEB) calculations, we located the transition state for the diffusion of the adsorbed hydrogen atom to bond with the O atom of the Nb-O-C linkage of ethoxy to form adsorbed ethanol specie, with an energy barrier of 0.38 eV. The second hydrogen atom also favors bonding to O_{2C} beside the Nb-O bond of adsorbed butyrate, and diffuses onto the O atom of the Nb-O-C linkage of adsorbed butyrate to form butyric acid species, the energy barrier is 0.77 eV. The third hydrogen atom adsorbs and helps to break the C-O bond of adsorbed ethanol with energy barrier of 0.29 eV, which result in the formation and desorption of ethane, leaves a H atom adsorb on surface O_{2C} (Figure S12)



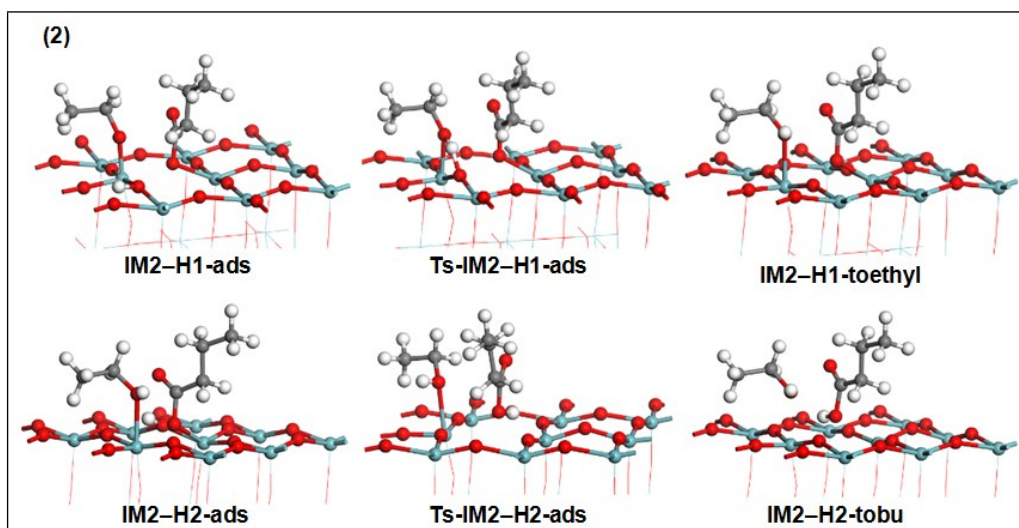
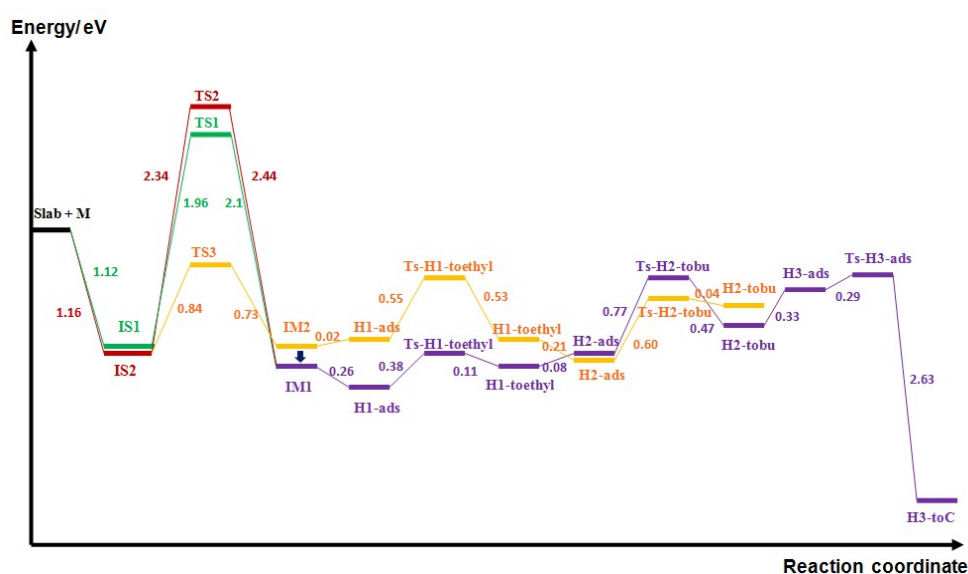


Figure S12. Calculated structures in the hydrogenation process of intermediate state IM1 (1) and IM2 (2). The Nb atoms are shown in light blue, O in red, C in black, and H in white.

For intermediate structure IM2, the first hydrogen atom prefers bond to O_{2C} beside the Nb-O bond of adsorbed ethoxy with adsorption energy of 0.02 eV. It diffuses to the O atom of the Nb-O-C linkage of adsorbed ethoxy to form adsorbed ethanol specie, with energy barrier of 0.55 eV. The second hydrogen atom bond to O_{2C} beside the Nb-O bond of adsorbed butyrate with adsorption energy of -0.21 eV, and diffuse onto the O atom of the Nb-O-C linkage of adsorbed butyrate, forming a structure of butyric acid adsorbed on oxygen vacancy, the energy barrier is 0.60 eV. We believe this structure makes the subsequent acid reduction process easy to happen. The corresponding energy profile is illustrated in Scheme 2.



Scheme 2. Calculated energy profile of the adsorption, dissociation and hydrogenation processes of ethyl butyrate on the $Nb_2O_5(001)$ surface.

Proposed structural changes during catalysis:

At this stage, it may be very difficult to elucidate the degree of surface oxygen vacancies in the glassy (amorphous) nature of Pd/NbOPO₄ because of the absence of defined crystalline surface and composition. XPS did not detect much change in Nb 3d peaks however, according to our TPR and EXAFS analysis, a significant degree of lattice oxygen in proximity of Pd nanoparticle can be extracted from this material in H₂. Thus, one would expect that the oxygen vacancies could be unevenly distributed on the material surface, which could be higher in concentration at the Pd/NbOPO₄ interface. During catalysis in liquid phase, the oxygen-containing molecules such as acids, alcohols and water can also replenish some of these surface oxygen vacancies. Thus, a dynamic equilibrium for the oxygen vacancies may exist on the surface. Nevertheless, we can rule out the direct formation of oxygen vacancy from the glassy phase without Pd, as evidenced by our DFT calculations that the oxygen vacancy formation energy was calculated to be as high as 3.68 eV.

It is noted that EXAFS as well as TPR are bulk techniques. Although they clearly indicated the formation of oxygen vacancies (i.e. from the change in bond lengths by EXAFS) from bulk material surface change may not be directly linked. As discussed above, we can rule out the direct formation of oxygen vacancy from the glassy phase without Pd, as evidenced by our DFT calculations that the oxygen vacancy formation energy was calculated to be as high as 3.68 eV. The presence of Pd nanoparticle at the material interface was also experimentally found to be crucial in the catalysis (see entry 6, Table 1). It is thus believed that the presence of Pd nanoparticle plays an important role in activation of H₂ on the surface to cause the bulk reduction of the NbOPO₄ phase observed by the EXAFS and TPR. This must be accomplished with the fast oxygen transfer from bulk to surface within the glassy NbOPO₄ phase at the material interface to give the observed room temperature reduction. As a result, the results thus suggest that the surface oxygen vacancies are in dynamic states with the bulk during the catalysis.

Reference

- [1] Y. Zhang, J. J. Wang, J. W. Ren, X. H. Liu, X. C. Li, Y. J. Xia, G. Z. Lu, Y. Q. Wang, *Catal. Sci. Technol.* **2012**, *2*, 2485-2491.
- [2] H. Yu, H. Fang, H. Zhang, B. Li, F. Deng, *Catal. Commun.* **2009**, *10*, 920-924.
- [3] H. Zhang, H. Yu, A. Zheng, S. Li, W. Shen, F. Deng, *Environ. Sci. Technol.*, **2008**, *42*, 5316-5321.
- [4] J. Yang, A. Zheng, M. Zhang, Q. Luo, Y. Yue, C. Ye, C. X. Lu, F. Deng, *J. Phys. Chem. B*, **2005**, *109*, 13124-13131.